

FRAME-C: A knowledge-augmented deep learning pipeline for classifying multi-electrode array electrophysiological signals

Nisal Ranasinghe¹, Dzung Do-Ha², Simon Maksour², Tamasha Malepathirana¹, Sachith Seneviratne¹,
Lezanne Ooi^{2*}, Saman Halgamuge^{1*}

¹AI, Optimization and Pattern Recognition Research Group, Dept. of Mechanical Eng.,
University of Melbourne, Australia

² Illawarra Health and Medical Research Institute, School of Biological Sciences, Faculty of Science,
Medicine and Health, University of Wollongong, Australia

* Correspondence - lezanne@uow.edu.au, saman@unimelb.edu.au

Abstract—Amyotrophic lateral sclerosis (ALS) is a fatal neurodegenerative disorder characterized by motor neuron degeneration, with alterations in neural excitability serving as key indicators. Recent advancements in induced pluripotent stem cell (iPSC) technology have enabled the generation of human iPSC-derived neuronal cultures, which, when combined with multi-electrode array (MEA) electrophysiology, provide rich spatial and temporal electrophysiological data. Traditionally, MEA data is analyzed using handcrafted features based on potentially imperfect domain knowledge, which while useful may not fully capture all the useful characteristics inherent in the MEA data. Machine learning, in particular deep learning has the potential to automatically learn relevant characteristics (features) from raw data, without solely relying on handcrafted feature extraction. However, handcrafted features remain critical for encoding domain knowledge and improving model interpretability, especially in scenarios with limited or noisy data, as is often the case in most experimental studies. This study introduces FRAME-C, a knowledge-augmented machine learning pipeline that combines domain knowledge, raw spike waveform data, and deep learning techniques to classify MEA signals and identify ALS-specific phenotypes. FRAME-C leverages deep learning to learn important features from spike waveforms, while also incorporating handcrafted features such as spike amplitude, inter-spike interval, and spike duration, thus preserving key spatial and temporal information. We validate FRAME-C on both simulated and real-world MEA data from human iPSC-derived neuronal cultures, demonstrating its superior performance compared to existing methods for MEA classification. FRAME-C performs significantly better, showing more than a 11% improvement on real-world data and up to 25% improvement on simulated data in terms of the test accuracy. Moreover, we show that FRAME-C can be used to evaluate the importance of each of the handcrafted features, and thereby contributing to the interpretation of the classification results. Permutation feature importances are calculated for these handcrafted features, providing further insights into the phenotypes of ALS.

Index Terms—Amyotrophic Lateral Sclerosis, Multi-electrode arrays, Knowledge augmentation, deep learning

I. INTRODUCTION

Amyotrophic lateral sclerosis (ALS) is a fatal neurodegenerative disease that leads to a progressive loss of motor neurons. At the onset of ALS, symptoms may include limb weakness and difficulty in swallowing. However, the disease invariably progresses towards paralysis and respiratory failure within three to five years [1].

A small portion of ALS patients (5 - 10%) are familial (fALS) in nature and can be linked to a family history of ALS. However, the majority (90 - 95%) are sporadic (sALS) and do not have any known family history. Many studies have been conducted on fALS to identify genes that contribute to the disease [2]–[5], and more than 30 genes have been linked to fALS [6], with many more believed to be unknown. While fALS has been well studied using mouse models,

this is not possible for sALS since there aren't any gene mutations linked to it.

Superoxide dismutase 1 (SOD1) is the best understood gene mutation that causes fALS, and was one of the first fALS genes identified in early studies. For more than two decades, the primary method of studying ALS was the SOD1 mouse model [7], a genetically modified mouse which carries a mutated version of the SOD1 gene. Although the mouse model has been a valuable tool in understanding ALS [8], there is much debate on its actual usefulness in understanding ALS [9]. Reasons include the doubts on how much the mouse model results would translate to humans, and the generalizability of SOD1 to other variants of ALS. SOD1 mutations only account for around 20% of fALS cases, which translates to only around 2-3% of all ALS cases

Human induced pluripotent stem cell technology (iPSC) provides another platform to study motor neuron diseases [10], [11]. They allow the development of neuronal cultures which mimic the structure of neurons. Since the neuron cultures are derived from human stem cells, they are a powerful model for studying both fALS and sALS.

In this work, we are particularly interested in the study of ALS electrophysiology. Changes in excitability through the disease progression is a well documented feature in ALS [12]–[14], and ALS patient iPSC-derived neuron cultures provide the opportunity to better study the excitability of ALS diseased neurons.

Multi-electrode arrays (MEA) allow the recording of electrophysiological signals within *in vitro* neuronal cultures. They consist of multiple electrodes that can simultaneously detect changes in extracellular voltage when neurons fire action potentials. Since each electrode records the activity from different regions of the neuronal culture with high resolution, MEAs provide rich information about both the timing (temporal resolution) and location (spatial resolution) of neural activity. When these MEAs are used with iPSC-derived neuronal cultures, they provide a powerful platform to study disease specific phenotypes in neuronal activity [15].

However, the richness of information in MEA data introduces many challenges in understanding and analyzing the data. The high dimensionality of MEA recordings make it challenging to analyze using manual or semi-automated processes. Traditionally, MEA signals are analyzed by extracting predefined features from the recording such as, and performing statistical analysis on these features [16]. “Spikes”—rapid changes in electrical activity that indicate neuron firing—are considered the most informative aspect of MEA data. Traditional methods focus on spike timing and firing rates, which are believed to capture the majority of the useful phenotypes that describe of cell behaviour and network dynamics. However, relying on predefined features limits the ability to fully leverage the detailed spatial and temporal information present in MEA recordings. The advancements of machine learning, in particular deep learning provide a powerful

alternative to learn the complex relationships within these high dimensional MEA datasets [17]–[19]. Deep learning methods generally do not rely on handcrafted features, since they can automatically extract latent features from unstructured raw data such as images, time series and text [20]. These models have achieved state-of-the-art results in various domains, demonstrating their potential for analyzing complex MEA signals.

In this work, we introduce Feature-based Raw data Augmentation for Multi-electrode array recorded Electrophysiological signal Classification (FRAME-C), a machine learning pipeline for classifying MEA signals based on electrophysiological phenotypes. FRAME-C combines domain knowledge with deep learning by integrating handcrafted features into the deep learning pipeline. We validate this pipeline on both simulated MEA data and in vitro MEA data obtained from human iPSC-derived neuronal cultures. To the best of our knowledge, this study represents the first application of deep learning methods to classify MEA recordings in the context of ALS research.

The main contributions of this paper are,

- 1) A knowledge augmentation method to integrate domain knowledge into deep learning methods for more accurate classification
- 2) FRAME-C: a machine learning pipeline that uses knowledge augmentation, data augmentation and deep learning to classify MEA signals
- 3) A detailed analysis of how each component of the pipeline affects the classification performance of FRAME-C

In Section II, we review the related literature on electrophysiological analysis, with a particular focus on MEA recordings and machine learning. Then, in Section III we introduce the datasets that we use for evaluating FRAME-C, including a simulated dataset and real-world MEA data recorded from human iPSC-derived neuronal cultures. In Section IV we introduce FRAME-C and discuss the components of the ML pipeline. The results of the conducted experiments are then presented in Section V followed by a summary of the work, limitations and future research directions in Section VI.

II. RELATED WORK

Machine learning methods have been used to perform predictive analytics using electrophysiological signals such as Electroencephalography (EEG) [21], Electrocardiography (ECG) [22] and Electromyography (EMG) [23]. However, there are only a few studies which explore the use of ML techniques in the study of MEA electrophysiology.

Traditionally, MEA data is analyzed by extracting features from action potentials and performing statistical analysis on them. Some commonly used features include mean firing rate (MFR), mean bursting rate (BR), network bursting rate (NBR) and burst duration (BD). Such analysis of MEA data has been shown to be a powerful tool in studying disease specific phenotypes [15]. However, these methods do not make full use of the rich spatial and temporal data in MEA recordings, since they can only study the pre-defined features that were extracted from the signals.

Buccino et al. proposed a deep learning pipeline for classification and localization of neurons using extracellular simulations. In this work, simulated waveforms are used to train a convolutional neural network (CNN) to predict the type and location of a neuron based on their extracellular action potentials (EAP). Features extracted from the EAPs are used to create 2D feature maps, with each point in the feature map corresponding to the feature value recorded on a given electrode. Multiple feature maps are stacked to create a 3D feature map which is then fed into the CNN for training. However, since

each training sample corresponds to a single action potential, the network cannot learn from the rich temporal information in the data. Moreover, the method is only applied to simulated EAPs, and has not been shown to be effective on real MEA data.

Zhao et al. proposed a convolutional neural network (CNN) to classify in vitro MEA recordings [17]. The authors apply this CNN to classify different genotypes using mouse iPSC derived neurons and human iPSC derived neurons with Williams syndrome. Before passing into the CNN, spike detection is performed on each MEA recording to transform the signal into a binary signal where 1 represents a spike and 0 represents a lack of a spike. Though this network is shown to perform better than simple machine learning methods such as logistic regression, it can be argued that the spike detection step removes a lot of useful information from the signal, since the model only sees whether the neuron fired or not, and does not see any information related to the shapes of the spikes.

Though most of the current work on MEA classification rely on handcrafted features based on domain knowledge, deep learning methods in general do not require handcrafted features. The hallmark of deep learning is its ability to automatically learn features from data. By leveraging the spatial and temporal richness of MEA recordings, deep learning approaches have the potential to uncover patterns and interactions that may not be apparent through traditional feature extraction methods. However, handcrafted features still play a crucial role, especially in scenarios where data is limited or the interpretability of the model is important. These features, derived from domain expertise, can provide insights into specific characteristics of the data that may guide the model's learning process. Additionally, combining handcrafted features with deep learning models can often enhance performance by incorporating prior knowledge, ensuring that the model captures both known and latent patterns in the data. The integration of domain knowledge with deep learning is known as knowledge augmentation (KA) [24].

III. DATASET

We evaluate our ML pipeline using two datasets.

- MEA data recorded from human iPSC derived neuronal cultures
- MEA data simulated using layer 5 cortical neuronal models

A. Human iPSC-derived neuronal culture data

TABLE I
FDS

Cell line	Sex	Age
sALS 1	M	51
Healthy Control 1	M	50
sALS 2	M	46
Healthy Control 2	M	46
sALS 3	M	50
Healthy Control 3	M	52
sALS 4	F	82
Healthy Control 4	F	75

1) *Motor neuron differentiation*: Four sporadic ALS and four age- and sex-matched donor iPSC lines were utilised in this study (Table I). iPSCs were maintained as previously described in Maksour et al., 2024 [25]. Motor neuron progenitors (MNP) were differentiated as previously described in Du et al., 2015, and cryopreserved prior to terminal motor neuron differentiation. 48 well CytoView MEA plates were coated with 100 $\mu\text{g/mL}$ poly-D-lysine in PBS for 1 h at RT, followed by 3x PBS washes. Plates were then coated with matrigel overnight at 4 $^{\circ}\text{C}$. MNPs were plated as single cells onto the coated MEA plates at a density of 40,000 cells/well in motor

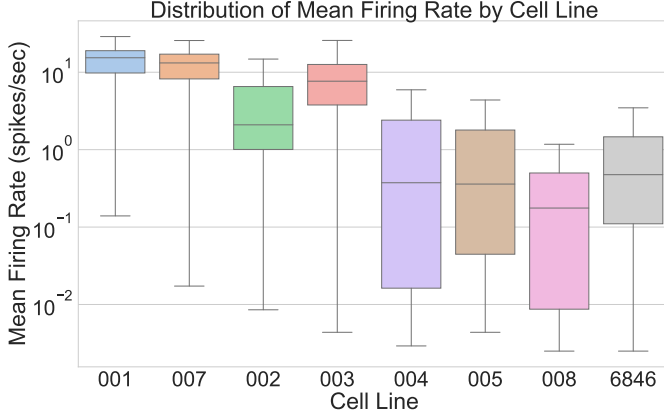


Fig. 1. The distribution of the mean firing rates of all the MEA signals recorded from human iPSC derived neuronal cultures. The MFR is shown on a log scale.

neuron media (BrainPhys, 1x N2 supplement, 1 x B27 supplement, 1x NEAA) supplemented with 10 ng/mL BDNF, GDNF, IGF, 500 ng/mL DB-cAMP, 200 ng/mL L-AA, 0.5 μ M retinoic acid, 0.1 μ M purmorphamine and 10 μ M DAPT, with half media changes every other day for the duration of MEA recording. Following 10 days of maturation, retinoic acid, purmorphamine and DAPT are removed from motor neuron media. Every second media change was supplemented with x μ g/mL laminin to promote cell adhesion.

2) *Microelectrode array measurements*: Motor neuron cultures were maintained for 1 week prior to recording spontaneous neuronal network activity using the Axion Maestro system. Recordings were performed at 37°C and 5% CO₂. Spontaneous neuronal network activity was recorded 3-4 times a week prior to media changes for 9 weeks. Electrophysiological data was acquired through the AxIS software (version 2.5) at a sampling rate of 12.5 kHz and passed through a high and low pass Butterworth filter (200 Hz – 3 kHz).

3) *Dataset exploration*: We perform exploratory analysis to further understand the dataset. The threshold crossing algorithm is used to detect action potentials in the recordings, which are then used to calculate the mean firing rates of the recordings. The mean firing rate *MFR* is defined as follows.

$$MFR = \frac{\sum_i^N spikes_i}{N * T} \quad (1)$$

Where N is the number of electrodes, $spikes_i$ is the number of spikes detected in the i th electrode, and T is the duration of the recording. The MFRs of all the MEA signals are illustrated using a box plot in Figure 1. We observed that the MFRs of the last four cell lines were significantly lower than the first four cell lines. This may have been due to changes in experimental factors, resulting in the neuronal cultures corresponding to those cell lines being less active when compared to the other cultures.

Cell lines 004, 005, 008 and 6846 which showed significantly lower spike counts were removed from the dataset since they would negatively impact the reliability of the analysis. These cell lines exhibited mean firing rates that were too low to provide meaningful insights into neuronal activity. Including such unreliable data could introduce noise and reduce the classifier’s ability to generalize.

B. Simulated data

To further evaluate the proposed pipeline, we simulate MEA recordings using the MEArec simulator [26]. MEArec is a fast, open-source Python based simulator to simulate MEA recordings.

It uses the NEURON simulation environment [27] for intracellular simulation which is then used for an extracellular simulation using the LFPy package [28]. This produces the extracellular action potentials generated at each electrodes location.

For simulating the MEA recordings, we use layer 5 (L5) cortical neuronal cell models from the Neocortical Microcircuit Portal [29]. This consists of 13 different cell models, some of which are inhibitory cells and the rest of which are excitatory cells. More details on the cell models used for the simulation are included in the supplementary materials. Each recording is simulated for 300 seconds with a sampling rate of 12500Hz. To better represent noisy MEA data, we add Gaussian noise to each recording of the simulated dataset.

Since we are interested in evaluating the performance of the proposed ML pipeline in it’s ability to distinguish between cell characteristics, two MEA recording datasets are simulated for each parameter configuration.

- Dataset 1 (Label 0) - Simulate with 10 excitatory cells
- Dataset 2 (Label 1) - Simulate with 10 inhibitory cells

IV. METHODS

Within this section, we introduce the ML pipeline and explain each component in detail. We first explain the pre-processing pipeline which extracts features and creates the dataset, and then the deep learning architecture that we use for classification. A detailed figure of the architecture of the ML pipeline is given in Figure 2.

A. Noise filtering and time split

We first apply a 4th order Butterworth filter with cut-off frequencies of 0.3 and 2KHz. Each signal is 300 seconds in length, and is sampled at 12500Hz. To increase the number of data samples, and to decrease the dimensionality of each sample, we split each signal into multiple smaller signals. Each time split signal is then considered as a single data sample.

B. Spike waveform extraction

The next step in the pipeline involves the detection of actions potentials (AP) and extracting the corresponding spike waveforms. AP detection, or spike detection was performed using the threshold crossing algorithm, with a threshold of 5 times the standard deviation of the noise level. The spike waveforms are captured by extracting 50 samples before and after the detected peak of the spike, yielding a waveforms of 100 samples per spike. Each waveform is represented by a 100 dimensional feature vector, corresponding to the voltage values of the spike over these 100 sample points. The full spike waveform captures the finer temporal details of the spike, which may not be captured by extracting handcrafted features like in traditional analysis. We expect the deep learning model to capture useful phenotypes of the spike using these raw waveforms.

C. Knowledge augmentation using spike features

Although deep learning models have been shown to be very successful in learning latent features from raw data, incorporating domain-specific handcrafted features can further enhance the model’s performance. We further augment the dataset using domain knowledge by extracting features from the detected spikes based and adding them to the spike waveform data. These features encode expert knowledge that may be challenging for the model to learn autonomously, especially from limited and noisy data. By adding these features, we also aim to improve the model’s interpretability. Having interpretable features allows us to later perform feature importance experiments to further understand the phenotypes that were

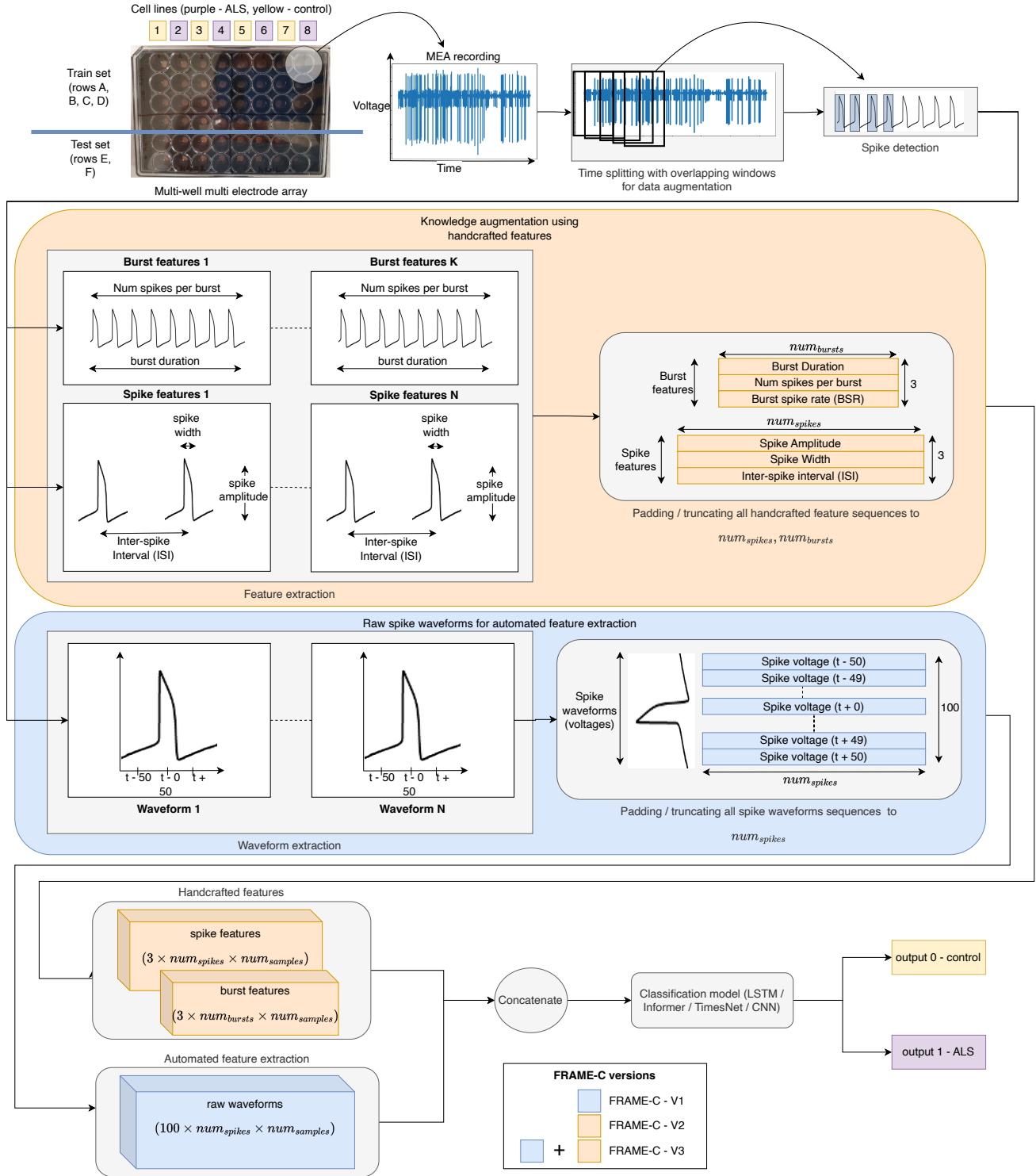


Fig. 2. The architecture of the proposed FRAME-C pipeline. The raw spike waveforms are augmented using handcrafted features based on domain knowledge. The sequences of spikes are truncated / padded to a fixed length of len_{spikes} , while the sequences of bursts are truncated / padded to a fixed length of len_{bursts}

useful for the model in classifying the MEA recordings. Moreover, handcrafted features can capture biologically relevant patterns that are not immediately obvious in raw data, that can lead to better generalization.tx

From each spike, the following features are extracted.

1) Spike amplitude: . This is the amplitude of a given AP. This is measured as the difference between the baseline noise level and the peak voltage value of the detected AP. Although the AP amplitude is not a commonly used feature in MEA analysis in ALS studies, it has been identified as a key feature in studies of other neurodegenerative

diseases such as Alzheimers [30].

2) *inter-spike interval (ISI)*: . This is the time interval between the AP and the next AP in the MEA signal. The ISI is a common phenotype used in MEA studies [15].

3) *Spike duration / spike width*: . This is width of the spike at half of the spike amplitude. We first identify the two points at which the MEA voltage is 50% of the maximum absolute voltage of the AP. The time interval between these two points is the spike duration, or the spike width [31].

Once the APs are detected, we further augment the dataset by detecting bursts, and corresponding burst related features. Bursts are regions in the MEA recording where a number of APs are fired within short intervals of each other, indicating regions of heightened excitability. Bursts that occur within a single channel of an MEA recording are known as single channel bursts. We detect single channel bursts by identifying consecutive APs with ISI values below a given min_{ISI} threshold. Moreover, we recognize such APs as bursts, only if they have at least min_{spikes} number of APs. We set min_{ISI} to 8ms and min_{spikes} to 4. Once the bursts are detected, we extract the following features.

4) *Burst duration*: . This is the time between the first and last AP of a given burst.

5) *Number of spikes*: . This is the total number of spikes in the burst.

6) *Burst spike rate (BSR)*: . This is the rate of firing of spikes within each burst. The BSR is calculated as $Burst\ duration / Number\ of\ spikes$.

Apart from spikes and single channel bursts, another commonly studied phenomenon in MEA recordings is network bursts [32]. A network burst occurs when multiple single channel bursts are recorded simultaneously across multiple electrodes. This is an indicator of network activity in the neuronal culture, where multiple neurons fire at once. In this study, we don't explicitly detect network bursts and extract network burst related features. This is because we don't remove the temporal information of the data when feeding it into the deep learning model. Therefore, we expect the deep learning model to capture any relevant network behaviour when training.

D. Creating feature sequences

Once spikes are detected, and the spike waveforms and features are extracted, feature sequences are created for each recording split. Each spike is represented using a concatenation of the spike waveform and the handcrafted features. Since the spike waveform consists of 100 data points, and there are three extracted spike features, this results in a 103-dimensional feature vector for each spike. This results in a feature sequence created for each recording split. When burst features are also included, we create a similar 3-dimensional feature sequence using just the extracted burst features. For example, if a recording split contains 2000 spikes, the spike feature sequence would be 103x2000. Similarly, for 200 bursts, the burst feature sequence would be of shape a 3x200.

To ensure uniformity across recordings with varying numbers of spikes and bursts, padding or truncation is applied, producing feature sequences of dimensions $103 \times n$ and $3 \times m$ where n is the fixed length of the spike sequences and m is the fixed length of the burst sequences. This approach preserves both temporal and spatial information while significantly reducing the dimensionality of the dataset, making it more efficient for subsequent analyses. By integrating both spike features and the waveform, the method achieves a balance between computational efficiency and the retention of biologically relevant signal characteristics, enhancing the overall quality of data representation for downstream tasks.

E. Deep learning model

Since the preprocessed dataset comprises of a sequence of features, we use deep learning architectures that are successful in learning relationships within sequences of data. We perform experiments with several deep learning architectures and compare their performance in accurately predicting the correct cell type.

1) *Long short term memory (LSTM) networks*: Recurrent neural networks (RNN) are a class of neural networks that are specifically designed to learn relationships in sequential data. RNNs have been applied in many fields such as natural language processing, time series analysis and even neuroscience [33]. The long short term memory (LSTM) network is a type of RNN that mitigates many of the problems of the vanilla RNN, allowing it to learn long term dependencies in long sequences of data. However, even LSTMs may fail in learning very long term dependencies in long sequences of data.

2) *Transformers and self-attention*: Transformers, a more recent and powerful architecture, have revolutionized sequence modeling by addressing some of the limitations of RNNs and LSTMs. Unlike recurrent models, transformers process entire sequences in parallel using "self-attention" mechanisms, enabling them to capture long-range dependencies efficiently. This architecture has been highly successful in tasks like natural language processing, protein structure prediction, and image recognition [34], [35]. Its ability to model global context without relying on sequential computation makes it a strong candidate for tasks involving complex sequential data. Although the transformer architecture was originally proposed for natural language processing tasks, it has rapidly been adopted in many fields which require the processing of sequential data, including time series data analysis.

Although transformers have mostly replaced LSTMs as the state-of-the-art architecture in natural language processing, and started to be adopted in many other fields, there is still evidence that RNNs and LSTMs still outperform transformer based methods in certain applications [36]. Transformers are computationally expensive and have a large number of parameters, and are therefore prone to overfitting, especially when trained on small datasets.

The power of transformers come at a high computational cost. The computational complexity of traditional self-attention scales quadratically with n , where n is the length of the sequence [37]. This makes it computationally infeasible for early transformer based architectures to learn from long time series data. However, more recent works have proposed improved transformer architectures that have lower computational complexities, allowing them to be trained on very long time series data. We are particularly interested in these type of models since the MEA data has can have long sequence lengths. The time series library [38], a recent benchmark for deep learning models specialized in time series data compares many state of the art models on various tasks. In our experiments, we use two deep learning models that are shown to achieve state-of-the-art results in time series classification.

Informer. The Informer architecture is designed to overcome the limitations of traditional transformers in modeling long sequence data, such as time series [39]. By introducing a probSparse self-attention mechanism, Informer reduces the computational complexity of the self-attention operation from $O(n^2)$ to $O(n \log n)$, where n is the sequence length. This sparsity mechanism selects only the most informative queries for attention calculations, allowing Informer to process long sequences efficiently without sacrificing performance. Additionally, it incorporates a distillation module that hierarchically compresses the input sequence, retaining only essential features and reducing redundancy. These innovations make Informer a highly efficient and scalable architecture, well-suited for tasks such as time

series forecasting and anomaly detection. Informer has demonstrated strong performance on various long sequence tasks, showcasing its utility in handling time series data with high dimensionality.

TimesNet. TimesNet is an architecture developed to address the challenges of learning from time series data with diverse temporal patterns [40]. Instead of relying on self-attention mechanisms, TimesNet employs a multi-scale convolutional framework to capture both localized and global temporal features. This approach allows it to efficiently model short-term fluctuations and long-term trends, which are critical for tasks like forecasting and classification. TimesNet also incorporates domain-specific priors, such as seasonal and periodic components, directly into its architecture, enhancing its ability to handle time series with strong temporal structures. Its modular design ensures scalability and interpretability, making it a practical choice for real-world applications. Benchmark evaluations have shown that TimesNet achieves state-of-the-art results on various time series tasks, offering a compelling alternative to transformer-based methods.

F. Data Augmentation

Deep learning models perform better when they are trained on large amounts of data. Although it's possible to generate as much data as needed when simulating recordings, collecting more real-world data in the form of MEA recordings is not always feasible. This is a common challenge with many deep learning models which rely on labelled datasets for training. Data augmentation is a technique used to artificially create more data from existing data, so that the ML model can be trained on a larger dataset.

As discussed earlier, we perform a time splitting of the MEA recording, since each recording is 300 seconds long. To further augment the size of the data, we perform a time split with a sliding window. The sliding window approach involves dividing the 300-second recordings into overlapping segments, where each window has a fixed duration (e.g., 10 seconds) and slides forward by a predetermined step size (e.g., 5 seconds). This method ensures that the entire recording is covered multiple times, creating overlapping segments that capture temporal continuity while enriching the dataset with more training samples. The overlap allows the model to learn subtle temporal patterns by exposing it to slightly shifted versions of the same data. This augmentation technique is particularly effective in retaining the contextual dynamics of the original recordings, thereby improving the robustness and generalization of the model trained on these enhanced datasets.

G. Batch effects observed

Batch effects refer to variations in a dataset caused by differences in technical or experimental conditions rather than biological differences. These variations, known as "non-biological variations," pose challenges for analyzing data with multiple batches. Factors that contribute to batch effects include differences in electrode sensitivity, sample preparation, and environmental conditions. Since ALS MEA data is generated using a multi-well MEA system, some degree of batch effects is expected in each well.

To investigate batch effects in the ALS dataset, we applied Uniform Manifold Approximation and Projection (UMAP) [41] to reduce the dataset's dimensionality and visualize the results in two dimensions. Each feature sequence was first flattened into a $k \times 1$ array, where k represents the total number of features. UMAP then reduced the data to two dimensions, which were visualized as a scatter plot. To assess the presence of batch effects, the points in the scatter plot were colored by the well number, allowing us to identify clusters based on the originating MEA wells. In the absence of batch effects, colors

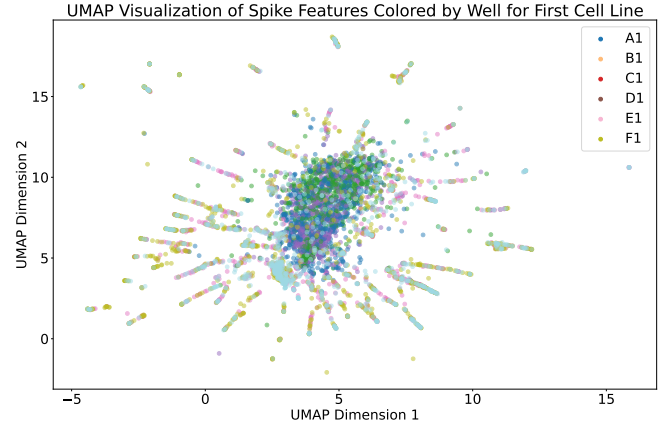


Fig. 3. The UMAP visualization of one of the ALS datasets, colored by the well number from where the MEA signal was recorded from. Some clusters are visible, which indicates that some batch effects are present in the dataset

in the scatter plot would be randomly distributed, with no visible clusters.

The UMAP visualization of data recorded at 36 days of maturation is shown in Figure 3. To simplify the visualization, we present only the wells corresponding to a single cell line, as including all wells would result in an overly complex plot. The figure reveals clustering patterns associated with the originating wells, indicating the presence of batch effects in the dataset. Notably, similar clustering patterns were observed across datasets from all wells and at different maturation stages, further confirming the widespread presence of batch effects in the data.

H. Wellwise train-test split

When creating a train-test split for training and evaluating the model, we considered two strategies. 1. Random split 2. Well-wise split. The random split involves randomly selecting a percentage of data samples for training and the rest for testing. However, this would mean that the model would see data from the same well during both training and testing. This gives rise to the possibility of the model relying on well-specific patterns (created due to batch effects) when performing the classification, leading to an overestimation of performance. To account for the batch effects observed in the ALS dataset, we instead chose a wellwise train-test split, meaning that data samples from the same well are kept entirely within either the training or testing set. This ensures that the model does not see data from the same well during both training and testing. By splitting the data wellwise, we ensure that the evaluation reflects the model's ability to generalize to data from wells it has not seen before, providing a more accurate assessment of its performance.

In our experiments we use well rows A, B, C, D for training and rows E, F for testing.

I. Model Evaluation

The real-world MEA dataset comprises an equal number of ALS and control cell lines, resulting in a balanced dataset. This balance justifies the use of accuracy as the evaluation metric, defined as the proportion of correctly classified samples across both classes. By ensuring equal representation of both classes, the dataset avoids class imbalance bias, providing a clear and reliable measure of the model's predictive performance. Accuracy is defined as follows.

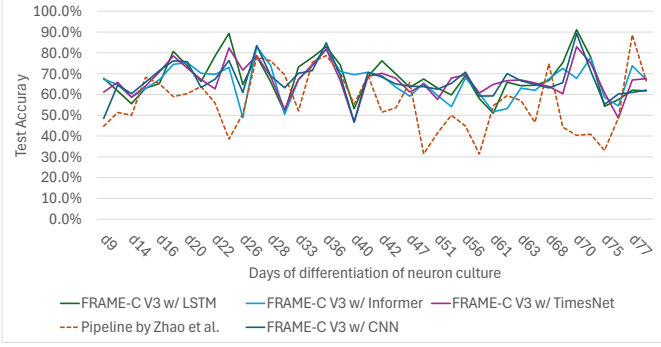


Fig. 4. The figure shows the change in test accuracy for each model versus the age of the neuronal culture

$$accuracy = \frac{\text{correctly_classified_count}}{\text{total_sample_count}} \quad (2)$$

The CNN-based method proposed by Zhao et al. employs a different time-splitting strategy than the one used in our proposed ML pipeline. Consequently, directly comparing accuracy values does not provide a like-for-like comparison, as the methods are evaluated on recording splits of differing sizes. To address this, we use a voting method to generate predictions for full recordings (300 seconds each). Specifically, predictions are generated for each time split within a recording, and the classification most frequently occurring across the splits is assigned to the entire recording. For instance, if a recording contains 20 time splits, of which 15 are classified as ALS and 5 as healthy, the overall classification for that recording would be ALS.

V. RESULTS AND DISCUSSION

The human iPSC-derived neuronal culture dataset consists of recordings taken on 40 different days, spanning maturation periods from 9 to 78 days. For each dataset, independent classification models were trained and tested, with test accuracies recorded for comparison. We evaluate 4 variations of FRAME-C, where each variation uses a different deep learning architecture for classification. These are 1) Informer [39], 2) TimesNet [40], LSTM and CNN. We compare these against the CNN-based MEA classification pipeline proposed by Zhao et al. [17]. To the best of our knowledge, this pipeline is the only other deep learning based pipeline for MEA classification that has been evaluated on *in vitro* MEA data. To obtain a fair comparison, we perform data augmentation for all methods by a factor of 10, including the pipeline proposed by Zhao et al.

To comprehensively evaluate the effect of the FRAME-C pipeline and knowledge augmentation, we conduct multiple experiments for each classification model and present the results in Table II. We report the mean test accuracies achieved by each method, calculated by averaging the test accuracy values across all 40 datasets.

Raw MEA recordings: In the first experiment, we train each model on raw MEA recordings to establish a baseline classification performance without any handcrafted features for incorporating domain knowledge. Only bandpass filtering and normalization are applied as preprocessing steps. Therefore, we rely on the deep learning models ability to automatically extract features from the raw MEA signal. As shown in the results, none of the models perform well, with all classifiers achieving just above 50% accuracy—only marginally better than random classification. The high dimensionality of raw MEA recordings, with relevant information concentrated in spikes, makes it challenging for even state-of-the-art time series classification models to extract useful features without domain-knowledge-informed preprocessing.

Pipeline by Zhao et al.: In the second experiment, we evaluate the pipeline proposed by Zhao et al. [17]. This approach uses spike extraction and dimensionality reduction through binning, preserving only the presence and absence of spikes while discarding spike characteristics. Since this pipeline was originally designed for a CNN classifier, we only evaluate it with that model, achieving an accuracy of 56.42%. Although this method shows an improvement over the baseline, the absence of spike characteristics may limit its ability to capture finer details relevant for classification.

FRAME-C V1: Next, we evaluate the FRAME-C pipeline using only spike waveforms for automated feature extraction. This approach leads to a substantial improvement in classification accuracy across all models, with a peak accuracy of 63.09%. Compared to raw MEA recordings, the inclusion of spike waveforms enhances model performance by providing temporal information, thus enabling deep learning models to extract more informative features. These results also surpass those obtained with the pipeline proposed by Zhao et al., highlighting the importance of spike characteristics for classification beyond merely detecting spike presence.

FRAME-C V2: We then evaluate the FRAME-C pipeline using only handcrafted features. This configuration incorporates domain knowledge by using handcrafted spike features and extracted spikes that provide temporal information, without performing any automated feature extraction. This approach yields further improvements, achieving gains of 2–3% over the experiments that used only spike waveforms. These results indicate that while deep learning models can effectively learn from spike waveforms, handcrafted features capture additional relevant information that enhances classification accuracy.

FRAME-C V3: In the final experiment, we evaluate the complete FRAME-C pipeline, which combines both spike waveforms for automated feature extraction and handcrafted spike features. This configuration achieves the highest classification accuracy across all models, demonstrating the complementary nature of the two feature types. Handcrafted features capture key statistical and morphological properties, while deep learning models extract additional patterns from the sequence of spike waveforms. These findings highlight the effectiveness of knowledge augmentation in enhancing class differentiation and underscore the importance of domain-knowledge-driven preprocessing in the FRAME-C pipeline.

A. Performance variation across maturation days

Figure 4 illustrates the performance variation of each model across datasets recorded at different maturation days. To maintain clarity and avoid an excessive number of results, only V3, the highest-performing version, is included. FRAME-C based methods demonstrate consistent performance improvements across all maturation stages compared to the pipeline proposed by Zhao et al.

B. Feature importances

To further investigate the influence of individual features on model performance, we conducted permutation feature importance experiments across all datasets. These experiments aimed to quantify the contribution of each handcrafted feature by assessing the decrease in model accuracy a single feature is removed while keeping other features intact. By applying this technique to our ML pipeline, we identified key features that significantly impacted classification accuracy. We perform the feature importance experiment on both the simulated and real-world MEA datasets.

For each feature k we train and evaluate FRAME-C with that feature removed. If the test accuracy when feature k is removed is given as acc_k , the feature importance is given by

TABLE II

THE EFFECT OF USING HANDCRAFTED FEATURES TO SUPPORT AUTOMATED FEATURE EXTRACTION BY DEEP LEARNING METHOD. TO EVALUATE FRAME-C, EXPERIMENTS WERE PERFORMED WITH DIFFERENT LEVELS OF AUTOMATED FEATURE EXTRACTION AND HANDCRAFTED FEATURES. THE PERFORMANCES ARE COMPARED IN TERMS OF THE TEST ACCURACY

Classification Pipeline	Automated feature extraction	Handcrafted features (provides domain knowledge)	Deep learning Classifier			
			Informer	TimesNet	CNN	LSTM
Raw MEA recording	Yes	No	53.34%	53.09%	N/A ¹	50.96%
Pipeline by Zhao et al.	No	Spike locations encoded as a binary sequence. No spike features.	N/A ²	N/A ²	56.42%	N/A ²
FRAME-C V1 (waveforms only)	Yes - from spike waveforms	No	57.71%	62.47%	63.09%	62.29%
FRAME-C V2 (handcrafted features only)	No	Handcrafted spike features	64.73%	65.12%	66.21%	66.45%
FRAME-C V3 (waveforms and handcrafted features)	Yes - from spike waveforms	Handcrafted spike features	65.92%	66.76%	66.66%	67.78%

¹ This experiment could not be conducted since it consumed over 150GB of memory.

² These experiments were not conducted since the pipeline by Zhao et al. was originally proposed with a CNN classifier.

TABLE III

THE EFFECT OF EACH HANDCRAFTED FEATURE IN THE CLASSIFICATION OF ALS MEA RECORDINGS. THE PERMUTATION FEATURE IMPORTANCE IS CALCULATED AS THE DROP IN PERFORMANCE WHEN THE CORRESPONDING FEATURE IS REMOVED FROM THE DATASET

Feature	Permutation feature importance
Inter-spike interval	12.30%
Spike amplitude	2.90%
Num spikes per burst	1.10%
Spike duration	0.80%
Burst spike rate	0.40%
Burst duration	-1.00%

TABLE IV

THE EFFECT OF EACH HANDCRAFTED FEATURE IN THE CLASSIFICATION OF SIMULATED MEA RECORDINGS.

Feature	Permutation feature importance
Spike duration	23.40%
Spike amplitude	1.60%
Inter-spike interval	0.00%
Burst duration	0.00%
/ Num spikes per burst	-0.50%
Burst spike rate	-1.00%

$$feature_importance_k = acc_{all} - acc_k \quad (3)$$

where acc_{all} is the accuracy when trained with all the features. The calculated feature importance scores for simulated data is given in IV and for the ALS MEA data is given in III. Since the ALS data and the simulated data do not reflect the same types of cells, we don't expect both of the datasets to yield similar feature importances.

For the simulated MEA data, spike duration emerged as the most critical feature, with a significant importance value of 23.40%, followed by spike amplitude at 1.60%. In contrast, features such as inter-spike interval and burst duration showed no measurable impact, and some features, like num spikes per burst and burst spike rate, even showed negative importance, suggesting redundancy or noise. For the ALS MEA data, inter-spike interval was the most influential feature, with an importance of 12.30%, followed by spike amplitude at 2.90%. Features like num spikes per burst and burst spike rate showed minor positive contributions, whereas burst duration had a slight negative importance.

For both datasets, a notable observation is that the burst related

features show little to no importance to the result. We note that all the information in the burst features are inherently available within the spike features. This is because the burst features are directly derived from spike related features. Therefore, we can reasonably assume that the model is successful in implicitly learning any burst related features that are relevant to the classification. Due to this observation, most later experiments were performed with the burst related features removed.

C. Effect of data augmentation

To further explore the impact of data augmentation by using overlapping time splits, we conducted additional experiments with and without data augmentation. Data augmentation is expected to enhance model performance by providing a more diverse set of training examples. We define the data augmentation factor α as the ratio of the size of the augmented dataset to the size of the original dataset. This can also be expressed in terms of the window size and step size as follows:

$$\alpha = \frac{\text{augmented data size}}{\text{original data size}} = \frac{\text{window size}}{\text{step size}} \quad (4)$$

In our experiments, we use an augmentation factor $\alpha = 10$, meaning the augmented dataset contains 10 times more samples than the original dataset. We train our machine learning pipeline on both the original and augmented datasets, and compare the test accuracies of the two configurations. The results of these experiments are shown in Table V. We observe a clear positive effect of data augmentation, with all tested methods demonstrating improved performance when trained on the augmented dataset.

D. Performance on simulated data

To further evaluate the performance of FRAME-C on a different type of dataset, we conducted experiments with FRAME-C to classify simulated MEA recordings. We use data simulated from L5 cortical neuronal models using MEARec [26], as outlined in Section III. The simulated recordings are generated using both inhibitory and excitatory cell models, and the models were trained to classify between these two classes of cells. To better mimic real-world data, Gaussian additive noise with a standard deviation of $20\mu V$ was added to the simulated recordings.

Multiple datasets of varying sizes were generated, and experiments were repeated on each dataset. For each experiment, we trained both

TABLE V

THE EFFECT OF DATA AUGMENTATION ON THE CLASSIFICATION PERFORMANCE. DATA AUGMENTATION IS ACHIEVED BY SPLITTING EACH RECORDING INTO MULTIPLE SEGMENTS WITH OVERLAPPING WINDOWS. THE OVERLAP IS CONFIGURED TO PRODUCE 10 TIMES MORE SAMPLES COMPARED TO NON-OVERLAPPING SPLITS. EACH METHOD IS EVALUATED BASED ON TEST ACCURACY.

Method	No data aug.	With data aug.
CNN classifier (Zhao et al. 2019)	57.24%	56.44%
FRAME-C V3 w/ Informer	63.27%	65.92%
FRAME-C V3 w/ TimesNet	65.74%	66.76%
FRAME-C V3 w/ CNN	66.28%	66.66%
FRAME-C V3 w/ LSTM	65.58%	67.82%

TABLE VI

PERFORMANCE COMPARISON OF FRAME-C V3 WITH LSTM AND THE PIPELINE BY ZHAO ET AL. ON SIMULATED MEA RECORDINGS. THE TABLE PRESENTS CLASSIFICATION ACCURACIES FOR DIFFERENT DATASET SIZES, MEASURED BY THE NUMBER OF SIMULATED WELLS (RECORDINGS) PER CELL TYPE. FRAME-C V3 WITH LSTM CONSISTENTLY OUTPERFORMS THE CNN-BASED METHOD BY ZHAO ET AL., WITH THE MOST SIGNIFICANT IMPROVEMENT OBSERVED ON SMALLER DATASETS.

Number of simulated wells (recordings) per cell type	Pipeline by Zhao et al.	FRAME-C V3 w/ LSTM
2	51.12%	75.06%
4	75.44%	82.05%
8	79.13%	84.58%
16	94.07%	94.21%

our ML pipeline and the CNN-based method proposed by Zhao et al. [17] and compared their test set accuracies. Since FRAME-C with LSTM performed the best in classifying the real-world ALS data, we use the LSTM classifier in these experiments. Moreover, we run the experiments using the highest performing version of the proposed pipeline, FRAME-C V3. To evaluate how each method performs on a datasets of different size, multiple experiments were performed with simulated datasets consisting of 2, 4, 8, and 16 simulated MEA recordings (each recording is 300 seconds long). Each recording would correspond to a single well in a multi-well MEA experiment. The results are shown in Table VI.

The results demonstrate that the proposed ML pipeline effectively distinguishes between cell types, consistently outperforming the CNN-based method by Zhao et al. This is more evident with smaller datasets, with a performance improvement of over 25% when trained on just two recordings, highlighting FRAME-C's ability to learn important phenotypes from the MEA recordings with limited and noisy data.

VI. CONCLUSION

In this work, we introduce FRAME-C, a machine learning pipeline that combines domain knowledge with raw signal data to classify MEA recordings. FRAME-C uses a spike detection algorithm to extract spike waveforms from the MEA recording, which are then fed into the deep learning model for automated feature extraction. Handcrafted features are used to incorporate domain knowledge into the pipeline, further improving classification performance. We evaluate FRAME-C on MEA data recorded from human iPSC-derived neuronal cultures in its ability to identify electrophysiological phenotypes in ALS by training it to classify between ALS-diseased and healthy cell lines. FRAME-C is shown to outperform existing methods, achieving up to an 11% improvement in test accuracy.

To further assess the robustness of FRAME-C, we evaluated its performance on simulated MEA data generated from cortical neuronal models. These experiments demonstrate FRAME-C's ability to generalize to a different type of dataset while maintaining strong classification performance. Notably, FRAME-C significantly outperformed the CNN-based approach by Zhao et al., particularly on smaller datasets, where it achieved a performance improvement of over 25% when trained on just two simulated recordings. This highlights FRAME-C's capability to extract meaningful phenotypic differences even from limited and noisy data.

Feature importance experiments reveal that the most discriminative feature varies depending on the dataset: spike duration is the most critical phenotype in classifying the simulated MEA data, whereas inter-spike interval (ISI) plays the most significant role in ALS classification. By leveraging domain-specific knowledge augmentation and advanced deep learning architectures, FRAME-C not only enhances classification accuracy but also provides interpretability by highlighting key phenotypic features.

Although FRAME-C demonstrates strong performance with both in-vitro and simulated multi-electrode array data, its generalizability to other types of electrophysiological data remains untested. Additionally, while the well-wise approach mitigates the misrepresentation of model performance caused by batch effects, the potential influence of such effects on overall performance cannot be ruled out. Future work may explore batch correction methods to further enhance the robustness and accuracy of FRAME-C.

ACKNOWLEDGEMENTS

This study was supported by the Melbourne Graduate Research Scholarship awarded to the first author. Additional support was provided by the FightMND Impact Grant 07 and the Department of Defense Therapeutic Ideas Award AL210047. Parts of this research were also supported by the Australian Research Council Centre of Excellence in Quantum Biotechnology (CE230100021, QUBIC). Computational resources were provided by the University of Melbourne's Research Computing Services and the Petascale Campus Initiative.

REFERENCES

- [1] R. H. Brown and A. Al-Chalabi, "Amyotrophic Lateral Sclerosis," *New England Journal of Medicine*, vol. 377, no. 2, pp. 162–172, Jul. 2017. [Online]. Available: <http://www.nejm.org/doi/10.1056/NEJMra1603471>
- [2] D. R. Rosen, T. Siddiquet, D. Patterson, D. A. Figlewicz, P. Sapp, A. Hentatit, D. Donaldson, J. Goto, J. P. O. H.-X. Dengt, Z. Rahmanit, A. Krizus, D. McKenna-Yasek, A. Cayabyabt, S. M. Gaston, R. Bergert, R. E. Tanzi, J. J. Halperin, B. Herzfeldt, R. Van den Bergh, W.-Y. Hungt, T. Birdt, G. Dengt, D. W. MulderH, C. Smytht, N. G. Laing, E. Sorianot, M. A. Pericak-Vancell, J. Haines, G. A. Rouleau, J. S. Gusella, H. Robert Horvitzll, and R. H. Brown Jr, "Mutations in Cu/Zn superoxide dismutase gene are associated with familial amyotrophic lateral sclerosis," *Tech. Rep.*, 1993.
- [3] A. E. Renton, E. Majounie, A. Waite, J. Simón-Sánchez, S. Rollinson, J. R. Gibbs, J. C. Schymick, H. Laaksovirta, J. C. van Swieten, L. Myllykangas, H. Kalimo, A. Paetau, Y. Abramzon, A. M. Remes, A. Kaganovich, S. W. Scholz, J. Duckworth, J. Ding, D. W. Harner, D. G. Hernandez, J. O. Johnson, K. Mok, M. Ryten, D. Trabzuni, R. J. Guerreiro, R. W. Orrell, J. Neal, A. Murray, J. Pearson, I. E. Jansen, D. Sondervan, H. Seelaar, D. Blake, K. Young, N. Halliwell, J. B. Callister, G. Toulson, A. Richardson, A. Gerhard, J. Snowden, D. Mann, D. Neary, M. A. Nalls, T. Peuralinna, L. Jansson, V. M. Isoviita, A. L. Kaivorinne, M. Hölttä-Vuori, E. Ikonen, R. Sulkava, M. Benatar, J. Wu, A. Chiò, G. Restagno, G. Borghero, M. Sabatelli, D. Heckerman, E. Rogaeva, L. Zinman, J. D. Rothstein, M. Sendtner, C. Drepper, E. E. Eichler, C. Alkan, Z. Abdullaev, S. D. Pack, A. Dutra, E. Pak, J. Hardy, A. Singleton, N. M. Williams, P. Heutink, S. Pickering-Brown, H. R. Morris, P. J. Tienari, and B. J. Traynor, "A hexanucleotide repeat expansion in C9ORF72 is the cause of chromosome 9p21-linked ALS-FTD," *Neuron*, vol. 72, no. 2, pp. 257–268, Oct. 2011.

- [4] M. DeJesus-Hernandez, I. R. Mackenzie, B. F. Boeve, A. L. Boxer, M. Baker, N. J. Rutherford, A. M. Nicholson, N. C. A. Finch, H. Flynn, J. Adamson, N. Kouri, A. Wojtas, P. Sengdy, G. Y. R. Hsiung, A. Karydas, W. W. Seeley, K. A. Josephs, G. Coppola, D. H. Geschwind, Z. K. Wszolek, H. Feldman, D. S. Knopman, R. C. Petersen, B. L. Miller, D. W. Dickson, K. B. Boylan, N. R. Graff-Radford, and R. Rademakers, "Expanded GGGGCC Hexanucleotide Repeat in Noncoding Region of C9ORF72 Causes Chromosome 9p-Linked FTD and ALS," *Neuron*, vol. 72, no. 2, pp. 245–256, Oct. 2011.
- [5] J. Sreedharan, I. P. Blair, V. B. Tripathi, X. Hu, C. Vance, B. Rogelj, S. Ackerley, J. C. Durnall, K. L. Williams, E. Buratti, F. Baralle, J. De Bellerocche, J. D. Mitchell, P. N. Leigh, A. Al-Chalabi, C. C. Miller, G. Nicholson, and C. E. Shaw, "TDP-43 Mutations in Familial and Sporadic Amyotrophic Lateral Sclerosis," *New Series*, vol. 319, no. 5870, pp. 1668–1672, 2008.
- [6] S. Chen, P. Sayana, X. Zhang, and W. Le, "Genetics of amyotrophic lateral sclerosis: an update," *Molecular Neurodegeneration*, vol. 8, no. 1, p. 28, Aug. 2013. [Online]. Available: <https://doi.org/10.1186/1750-1326-8-28>
- [7] J. Hawrot, S. Imhof, and B. J. Wainger, "Modeling cell-autonomous motor neuron phenotypes in ALS using iPSCs," *Neurobiology of Disease*, vol. 134, Feb. 2020, publisher: Academic Press Inc.
- [8] M. E. Gurney, H. Pu, A. Y. Chiu, M. C. Dal Canto, C. Y. Polchow, D. D. Alexander, J. Caliendo, A. Hentati, Y. W. Kwon, H.-X. Deng, W. Chen, P. Zhai, R. L. Sufit, and T. Siddique, "Motor Neuron Degeneration in Mice that Express a Human Cu,Zn Superoxide Dismutase Mutation," *Science*, vol. 264, no. 5166, pp. 1772–1775, Jun. 1994.
- [9] M. Benatar, "Lost in translation: treatment trials in the SOD1 mouse and in human ALS," *Neurobiology of Disease*, vol. 26, no. 1, pp. 1–13, Apr. 2007.
- [10] K. Takahashi and S. Yamanaka, "Induction of Pluripotent Stem Cells from Mouse Embryonic and Adult Fibroblast Cultures by Defined Factors," *Cell*, vol. 126, no. 4, pp. 663–676, Aug. 2006.
- [11] —, "A decade of transcription factor-mediated reprogramming to pluripotency," *Nature Reviews Molecular Cell Biology*, vol. 17, no. 3, pp. 183–193, Mar. 2016, publisher: Nature Publishing Group. [Online]. Available: <https://www.nature.com/articles/nrm.2016.8>
- [12] D. Do-Ha, Y. Buskila, and L. Ooi, "Impairments in Motor Neurons, Interneurons and Astrocytes Contribute to Hyperexcitability in ALS: Underlying Mechanisms and Paths to Therapy," *Molecular Neurobiology*, vol. 55, no. 2, pp. 1410–1418, Feb. 2018, publisher: Humana Press Inc.
- [13] B. J. Wainger, E. Kiskinis, C. Mellin, O. Wiskow, S. S. Han, J. Sandoe, N. P. Perez, L. A. Williams, S. Lee, G. Boulting, J. D. Berry, R. H. Brown, M. E. Cudkowicz, B. P. Bean, K. Eggan, and C. J. Woolf, "Intrinsic membrane hyperexcitability of amyotrophic lateral sclerosis patient-derived motor neurons," *Cell Reports*, vol. 7, no. 1, pp. 1–11, Oct. 2014, publisher: Elsevier.
- [14] Y. Buskila, O. Kékesi, A. Bellot-Saez, W. Seah, T. Berg, M. Trpcski, J. J. Yerbury, and L. Ooi, "Dynamic interplay between H-current and M-current controls motoneuron hyperexcitability in amyotrophic lateral sclerosis," *Cell Death and Disease*, vol. 10, no. 4, Apr. 2019, publisher: Nature Publishing Group.
- [15] B. Mossink, A. H. Verboven, E. J. van Hugte, T. M. Klein Gunnewiek, G. Parodi, K. Linda, C. Schoenmaker, T. Kleefstra, T. Kozicz, H. van Bokhoven, D. Schubert, N. Nadif Kasri, and M. Frega, "Human neuronal networks on micro-electrode arrays are a highly robust tool to study disease-specific genotype-phenotype correlations in vitro," *Stem Cell Reports*, vol. 16, no. 9, pp. 2182–2196, Sep. 2021, publisher: Cell Press.
- [16] A. Bryson, D. Mendis, E. Morrisroe, C. A. Reid, S. Halgamuge, and S. Petrou, "Classification of antiepileptic drugs in cultured neuronal networks using multielectrode arrays and unsupervised learning," *Epilepsia*, vol. 63, no. 7, pp. 1693–1703, 2022, eprint: <https://onlinelibrary.wiley.com/doi/pdf/10.1111/epi.17268>. [Online]. Available: <https://onlinelibrary.wiley.com/doi/abs/10.1111/epi.17268>
- [17] Y. Zhao, E. Guzman, M. Audouard, Z. Cheng, P. Hansma, K. S. Kosik, and L. Petzold, "A Deep Learning Framework for Classification of in vitro Multi-Electrode Array Recordings," Jun. 2019, arXiv: 1906.02241. [Online]. Available: <https://arxiv.org/abs/1906.02241>
- [18] A. P. Buccino, M. Kordovan, T. V. Ness, B. Merkt, P. D. Häfliger, M. Fyhn, G. Cauwenberghs, S. Rotter, and G. T. Einevoll, "Combining biophysical modeling and deep learning for multielectrode array neuron localization and classification," *Journal of Neurophysiology*, vol. 120, no. 3, pp. 1212–1232, Sep. 2018. [Online]. Available: <https://www.physiology.org/doi/10.1152/jn.00210.2018>
- [19] T. Malepathirana, D. Senanayake, V. Gautam, M. Engel, R. Balez, M. D. Lovelace, G. Sundaram, B. Heng, S. Chow, C. Marquis, G. J. Guillemain, B. Brew, C. Jagadish, L. Ooi, and S. Halgamuge, "Visualization of incrementally learned projection trajectories for longitudinal data," *Scientific Reports*, vol. 14, no. 1, p. 13558, Jun. 2024, publisher: Nature Publishing Group. [Online]. Available: <https://www.nature.com/articles/s41598-024-63511-z>
- [20] S. Dong, P. Wang, and K. Abbas, "A survey on deep learning and its applications," *Computer Science Review*, vol. 40, p. 100379, May 2021. [Online]. Available: <https://www.sciencedirect.com/science/article/pii/S1574013721000198>
- [21] M.-P. Hosseini, A. Hosseini, and K. Ahi, "A Review on Machine Learning for EEG Signal Processing in Bioengineering," *IEEE reviews in biomedical engineering*, vol. 14, pp. 204–218, 2021.
- [22] S. S. Al-Zaiti, C. Martin-Gill, J. K. Zègre-Hemsey, Z. Bouzid, Z. Faramand, M. O. Alrawashdeh, R. E. Gregg, S. Helman, N. T. Riek, K. Kraevsky-Phillips, G. Clermont, M. Akcakaya, S. M. Sereika, P. Van Dam, S. W. Smith, Y. Birnbaum, S. Saba, E. Sejdic, and C. W. Callaway, "Machine learning for ECG diagnosis and risk stratification of occlusion myocardial infarction," *Nature Medicine*, vol. 29, no. 7, pp. 1804–1813, Jul. 2023, publisher: Nature Publishing Group. [Online]. Available: <https://www.nature.com/articles/s41591-023-02396-3>
- [23] H. A. Yousif, A. Zakaria, N. A. Rahim, A. F. B. Salleh, M. Mahmood, K. A. Alfarhan, L. M. Kamarudin, S. M. Mamduh, A. M. Hasan, and M. K. Hussain, "Assessment of Muscles Fatigue Based on Surface EMG Signals Using Machine Learning and Statistical Approaches: A Review," *IOP Conference Series: Materials Science and Engineering*, vol. 705, no. 1, p. 012010, Nov. 2019, publisher: IOP Publishing. [Online]. Available: <https://dx.doi.org/10.1088/1757-899X/705/1/012010>
- [24] Z. Cui, T. Gao, K. Talamadupula, and Q. Ji, "Knowledge-Augmented Deep Learning and Its Applications: A Survey," *IEEE Transactions on Neural Networks and Learning Systems*, pp. 1–21, 2023, conference Name: IEEE Transactions on Neural Networks and Learning Systems. [Online]. Available: <https://ieeexplore.ieee.org/document/10359123/?arnumber=10359123>
- [25] S. Maksour, R. K. Finol-Urdaneta, A. J. Hulme, M. e. C. Cabral-da Silva, H. Targa Dias Anastacio, R. Balez, T. Berg, C. Turner, S. Sanz Muñoz, M. Engel, P. Kalajdzic, L. Lisowski, K. Sidhu, P. S. Sachdev, M. Dottori, and L. Ooi, "Alzheimer's disease induced neurons bearing PSEN1 mutations exhibit reduced excitability," *Frontiers in Cellular Neuroscience*, vol. 18, Oct. 2024, publisher: Frontiers. [Online]. Available: <https://www.frontiersin.org/journals/cellular-neuroscience/articles/10.3389/fncel.2024.1406970/full>
- [26] A. P. Buccino and G. T. Einevoll, "MEArc: A Fast and Customizable Testbench Simulator for Ground-truth Extracellular Spiking Activity," *Neuroinformatics*, vol. 19, no. 1, pp. 185–204, Jan. 2021, publisher: Springer. [Online]. Available: <https://link.springer.com/10.1007/s12021-020-09467-7>
- [27] N. T. Carnevale and M. L. Hines, *The NEURON Book*. Cambridge University Press, Jan. 2006.
- [28] H. Linden, E. Hagen, S. Leski, E. S. Norheim, K. H. Pettersen, and G. T. Einevoll, "LFPy: a tool for biophysical simulation of extracellular potentials generated by detailed model neurons," *Frontiers in Neuroinformatics*, vol. 7, 2014.
- [29] S. Ramaswamy, J. D. Courcol, M. Abdellah, S. R. Adaszewski, N. Antille, S. Arsever, G. Atnekeng, A. Bilgili, Y. Brukau, A. Chalimourda, G. Chindemi, F. Delalondre, R. Dumusc, S. Eilemann, M. E. Gevaert, P. Gleeson, J. W. Graham, J. B. Hernando, L. Kanari, Y. Katkov, D. Keller, J. G. King, R. Ranjan, M. W. Reimann, C. Rössert, Y. Shi, J. C. Shillcock, M. Telefont, W. Van Geit, J. Villafraña Diaz, R. Walker, Y. Wang, S. M. Zaninetta, J. DeFelipe, S. L. Hill, J. Muller, I. Segev, F. Schürmann, E. B. Muller, and H. Markram, "The neocortical micro-circuit collaboration portal: A resource for rat somatosensory cortex," *Frontiers in Neural Circuits*, vol. 9, no. OCT, Oct. 2015, publisher: Frontiers Research Foundation.
- [30] Y. Wang, G. Zhang, H. Zhou, A. Barakat, and H. Querfurth, "Opposite Effects of Low and High Doses of AB42 on Electrical Network and Neuronal Excitability in the Rat Prefrontal Cortex," *PLoS ONE*, vol. 4, no. 12, p. e8366, Dec. 2009. [Online]. Available: <https://dx.plos.org/10.1371/journal.pone.0008366>
- [31] K. Weir, O. Blanquie, W. Kilb, H. J. Luhmann, and A. Sinning, "Comparison of spike parameters from optically identified GABAergic and glutamatergic neurons in sparse cortical cultures," *Frontiers in Cellular Neuroscience*, vol. 8, p. 460, Jan. 2015. [Online]. Available: <https://www.ncbi.nlm.nih.gov/pmc/articles/PMC4294161/>
- [32] G. D. Mendis, E. Morrisroe, S. Petrou, and S. K. Halgamuge, "Use of adaptive network burst detection methods for multielectrode array data and the generation of artificial spike patterns for method evaluation,"

- Journal of Neural Engineering*, vol. 13, no. 2, Feb. 2016, publisher: Institute of Physics Publishing.
- [33] O. Barak, "Recurrent neural networks as versatile tools of neuroscience research," *Current Opinion in Neurobiology*, vol. 46, pp. 1–6, Oct. 2017. [Online]. Available: <https://www.sciencedirect.com/science/article/pii/S0959438817300429>
 - [34] A. Vaswani, G. Brain, N. Shazeer, N. Parmar, J. Uszkoreit, L. Jones, A. N. Gomez, L. Kaiser, and I. Polosukhin, "Attention Is All You Need," in *Advances in Neural Information Processing Systems*. Curran Associates, Inc., 2017.
 - [35] A. Dosovitskiy, L. Beyer, A. Kolesnikov, D. Weissenborn, X. Zhai, T. Unterthiner, M. Dehghani, M. Minderer, G. Heigold, S. Gelly, J. Uszkoreit, and N. Houlsby, "An Image is Worth 16x16 Words: Transformers for Image Recognition at Scale," Oct. 2020, arXiv: 2010.11929. [Online]. Available: <http://arxiv.org/abs/2010.11929>
 - [36] P.-A. Buestan-Andrade, M. Santos, J.-E. Sierra-García, and J.-P. Pazmiño-Piedra, "Comparison of LSTM, GRU and Transformer Neural Network Architecture for Prediction of Wind Turbine Variables," in *18th International Conference on Soft Computing Models in Industrial and Environmental Applications (SOCO 2023)*, P. García Bringas, H. Perez García, F. J. Martínez de Pisón, F. Martínez Álvarez, A. Troncoso Lora, A. Herrero, J. L. Calvo Rolle, H. Quintián, and E. Corchado, Eds. Cham: Springer Nature Switzerland, 2023, pp. 334–343.
 - [37] F. D. Keles, P. M. Wijewardena, and C. Hegde, "On The Computational Complexity of Self-Attention," Sep. 2022, arXiv:2209.04881 [cs]. [Online]. Available: <http://arxiv.org/abs/2209.04881>
 - [38] Y. Wang, H. Wu, J. Dong, Y. Liu, M. Long, and J. Wang, "Deep Time Series Models: A Comprehensive Survey and Benchmark," Jul. 2024, arXiv:2407.13278 [cs]. [Online]. Available: <http://arxiv.org/abs/2407.13278>
 - [39] H. Zhou, S. Zhang, J. Peng, S. Zhang, J. Li, H. Xiong, and W. Zhang, "Informer: Beyond Efficient Transformer for Long Sequence Time-Series Forecasting," *Proceedings of the AAAI Conference on Artificial Intelligence*, vol. 35, no. 12, pp. 11 106–11 115, May 2021, number: 12. [Online]. Available: <https://ojs.aaai.org/index.php/AAAI/article/view/17325>
 - [40] H. Wu, T. Hu, Y. Liu, H. Zhou, J. Wang, and M. Long, "TimesNet: Temporal 2D-Variation Modeling for General Time Series Analysis," Oct. 2022, arXiv: 2210.02186. [Online]. Available: <http://arxiv.org/abs/2210.02186>
 - [41] L. McInnes, J. Healy, and J. Melville, "UMAP: Uniform Manifold Approximation and Projection for Dimension Reduction," Feb. 2018, arXiv: 1802.03426.